

## Synthesis and Physical Properties of the New Layered Ternary Tellurides $M\text{IrTe}_4$ ( $M = \text{Nb}, \text{Ta}$ ), and the Structure of $\text{NbIrTe}_4$

ARTHUR MAR AND JAMES A. IBERS<sup>1</sup>

*Department of Chemistry and Science and Technology Center for Superconductivity, Northwestern University, Evanston, Illinois 60208-3113*

Received August 1, 1991

Two new ternary transition-metal chalcogenides, niobium iridium tetratelluride ( $\text{NbIrTe}_4$ ) and tantalum iridium tetratelluride ( $\text{TaIrTe}_4$ ), have been prepared by reaction of the elemental powders at 1000°C. The structure of  $\text{NbIrTe}_4$  has been determined by single-crystal X-ray diffraction methods. The compound crystallizes in space group  $C_{2v}^2-Pmn2_1$  of the orthorhombic system with four formula units in a cell of dimensions  $a = 3.768(3)$ ,  $b = 12.486(10)$ ,  $c = 13.077(9)$  Å at 294 K.  $\text{NbIrTe}_4$  is a layered compound with a structure closely related to those of  $\text{WTe}_2$  and  $\beta\text{-MoTe}_2$ , variants of the  $\text{CdI}_2$  structure type. The layers comprise buckled sheets of Te atoms, with the Nb and Ir atoms residing in distorted octahedral sites. Metal–metal bonding appears to be responsible for a close association of the Nb and Ir atoms. From Weissenberg photography, the compound  $\text{TaIrTe}_4$  is found to be isostructural to  $\text{NbIrTe}_4$ , with cell dimensions  $a = 3.77(3)$ ,  $b = 12.37(6)$ ,  $c = 13.17(3)$  Å. Electrical resistivity measurements along the  $a$  axis of both compounds show that they are metallic:  $\rho_{298} = 8.1 \times 10^{-5}$  and  $1.2 \times 10^{-4}$  Ω cm for  $\text{NbIrTe}_4$  and  $\text{TaIrTe}_4$ , respectively. Magnetic susceptibility measurements indicate essentially temperature-independent Pauli paramagnetism for both compounds:  $\chi_m = 1.9 \times 10^{-3}$  and  $8.9 \times 10^{-4}$  emu mol<sup>-1</sup> for  $\text{NbIrTe}_4$  and  $\text{TaIrTe}_4$ , respectively. The compounds  $\text{NbIrTe}_4$  and  $\text{TaIrTe}_4$  appear to belong to a larger class of compounds  $MM'\text{Te}_4$  with  $M = \text{Nb}, \text{Ta}$  and  $M' = \text{Ru}, \text{Os}, \text{Rh}, \text{Ir}$ . © 1992 Academic Press, Inc.

### Introduction

Traditionally, tellurides of the transition metals have received less attention than the sulfides and selenides, but efforts in this and more recently in other groups have revealed many new ternary tellurides, specifically of the early transition metals Zr, Hf, Nb, and Ta. In accord with its less ionic character, tellurium has a greater tendency to show a wide range of  $\text{Te}\cdots\text{Te}$  interactions, up to full Te–Te single bonds (1).

Many of these ternary tellurides readily adopt low-dimensional structures, sometimes as chains (e.g.,  $\text{Ta}_4\text{SiTe}_4$  (2),  $\text{K}_4\text{Hf}_3\text{Te}_{17}$  (3)), but more commonly as layers (e.g.,  $\text{Cu}_2\text{ZrTe}_3$  (4),  $\text{NbNiTe}_5$  (5),  $\text{Ta}_4\text{Pd}_3\text{Te}_{16}$  (6),  $\text{Ta}_2\text{Ni}_2\text{Te}_4$  (7),  $\text{Nb}_2\text{Ni}_2\text{Te}_4$  (8)). Although the structures of these compounds could not have been easily predicted, the simple notion of preferred coordination geometries of the transition metals is helpful in rationalizing known structures and providing ideas for new target compounds (9).

Prompted by the discovery of several  $MM'\text{Te}_5$  ( $M = \text{Nb}, \text{Ta}$ ;  $M' = \text{Ni}, \text{Pd}, \text{Pt}$ )

<sup>1</sup> To whom correspondence should be addressed.

compounds that comprise  $M$  bicapped trigonal prisms and  $M'$  octahedra (5, 10–12), we have attempted to extend these systems to other Pt-group metals  $M' = \text{Ru, Os, Rh, Ir}$  that also adopt octahedral geometries. Would they also form  $MM'Te_5$  phases?

Investigations in related selenide systems were recently undertaken toward the preparation of  $Ta_{1-x}M'_xSe_2$  ( $M' = \text{Re, Os, Ir, Pt}$ ), in order to determine the extent to which partial substitution of Ta with  $M'$  stabilizes its trigonal prismatic coordination (13). The only compounds prepared were  $Ta_{0.50}Re_{0.50}Se_2$  and  $Ta_{0.67}Os_{0.33}Se_2$ ; both show complete disorder of the metal atoms. While  $NbQ_2$  and  $TaQ_2$  ( $Q = \text{S, Se}$ ) occur in many polytypes in which Nb or Ta can be either trigonal prismatic or octahedral (14), only octahedral coordination is observed in the  $NbTe_2$  and  $TaTe_2$  systems (14, 15). Thus the corresponding ternary telluride systems can be expected to behave very differently.

In view of these observations on  $MM'Te_5$  and  $Ta_{1-x}M'_xSe_2$  we could not predict what phases might exist in the  $M/M'/Te$  ( $M = \text{Nb, Ta; } M' = \text{Ru, Os, Rh, Ir}$ ) systems. Here we report the preparation of two new ternary tellurides  $NbIrTe_4$  and  $TaIrTe_4$  that are related to *neither* of the two aforementioned systems, but rather to the binary tellurides  $WTe_2$  and  $\beta\text{-MoTe}_2$  (16). The structure of  $NbIrTe_4$  and the electrical resistivities and magnetic susceptibilities of  $NbIrTe_4$  and  $TaIrTe_4$  are described here.

## Experimental

**Synthesis.** The compound  $NbIrTe_4$  was prepared from a reaction of powders of the elements in an atomic ratio of Nb : Ir : Te = 1 : 1 : 8 (Nb, 18 mg, 0.19 mmol, 99.8%; Ir, 37 mg, 0.19 mmol, 99.95%; Te, 196 mg, 1.53 mmol, 99.999%; all from AESAR) that were ground together and loaded into a quartz tube (10-cm length, 4-mm ID) that was then evacuated ( $10^{-4}$  Torr). The tube

was placed in a furnace, heated at 500°C for 1 day, 800°C for 1 day, and 1000°C for 12 days, and then cooled to room temperature over 1 day. The sample consisted predominantly of a black powder that was identified to be a mixture of  $NbIrTe_4$ ,  $Ir_3Te_8$ , and  $NbTe_4$  from X-ray powder diffraction patterns obtained on an Enraf–Nonius FR522 Guinier camera. Excess Te and a few needles of  $NbTe_4$  were also present in this sample. The entire sample was reground and reheated at 1000°C for 4 days, and then slowly cooled at 10°/hr to room temperature. The product consisted of excess Te and a large irregular laminar aggregate of very soft, flat, shiny gray, needle-shaped crystals. A microprobe analysis of these crystals with an EDAX (Energy Dispersive Analysis by X-rays) equipped Hitachi S570 scanning electron microscope revealed the presence of all three elements in an atomic ratio of roughly Nb : Ir : Te = 1.0 : 1.2 : 4.0, in good agreement with the composition  $NbIrTe_4$  established from the X-ray crystal structure determination. Owing to the layered nature of the compound, these crystals are extremely pliable and very easily deformed, rendering them unsuitable for single-crystal X-ray diffraction experiments. The deformed crystals were used for magnetic susceptibility measurements, while better shaped crystals were reserved for electrical conductivity measurements. After numerous crystals were screened by Weissenberg photography, an untwinned, sharply-diffracting single crystal was selected for the crystal structure determination. Stoichiometric reaction of the elements usually fails to yield  $NbIrTe_4$ , as does the use of various transport agents ( $I_2$ ,  $TeBr_4$ ,  $TeCl_4$ ). An excess of Te appears to be necessary for its formation.

The compound  $TaIrTe_4$  was prepared from a reaction of powders of the elements in an atomic ratio of Ta : Ir : Te = 1 : 1 : 8 (Ta, 31 mg, 0.18 mmol, 99.98%, AESAR; Ir, 36 mg, 0.18 mmol, 99.95%, AESAR; Te,

184 mg, 1.43 mmol, 99.8%, Aldrich) ground together and loaded as described above. The tube was heated under the same temperature program as above to afford a gray powder containing mostly  $\text{Ir}_3\text{Te}_8$ , a small aggregate of thin needle-shaped crystals, and excess Te. EDAX measurements established the needles as the ternary compound  $\text{TaIrTe}_4$  (Ta:Ir:Te = 1.1:1.0:3.8). These crystals were used for electrical conductivity experiments. Other syntheses, starting from elements in an atomic ratio of Ta:Ir:Te = 1:1:8 and 1:1:12, heated to 1000°C for 3 days, and slowly cooled at ~8°C/hr to room temperature, yielded sufficient quantities of soft, easily-bent needles of  $\text{TaIrTe}_4$  for magnetic susceptibility measurements. Stoichiometric reactions and use of transport agents also fail in this instance.

*Electrical resistivity.* Single crystals of  $\text{NbIrTe}_4$  and  $\text{TaIrTe}_4$  ranging from 0.7 to 1.4 mm in length and  $2 \times 10^{-4}$  to  $1 \times 10^{-3}$  mm<sup>2</sup> in cross-sectional area were mounted with Ag paint on Al wires extended by graphite fibers. Because  $\text{NbTe}_4$  and  $\text{TaTe}_4$  are common impurities whose color and needle-shaped habit are easily confused with those of  $\text{NbIrTe}_4$  and  $\text{TaIrTe}_4$ , respectively, the integrity of the mounted crystals was first checked by EDAX measurements. The electrical resistivities along the needle axis *a* of  $\text{NbIrTe}_4$  and  $\text{TaIrTe}_4$  were then measured by a four-probe ac (27 Hz) phase-locked technique, as described previously (17). Samples were cooled at a rate of approximately 1 deg/min by use of a flow of cold helium gas. The uncertainties in the measurements of crystal dimensions lead to relative uncertainties in the resistivity values of  $(\Delta\rho)/\rho = \pm 0.2$ . The crystals are too thin to permit measurements of resistivity perpendicular to the needle axis.

*Magnetic susceptibility.* To ensure phase purity of the samples used for magnetic measurements, single crystals or aggregates of single crystals of  $\text{NbIrTe}_4$  and

$\text{TaIrTe}_4$  were manually selected. The compositions of randomly selected crystals from each sample were confirmed by EDAX measurements. The crystals were then ground to fine powders that were further identified by X-ray powder diffraction. The samples were reasonably pure, although a small amount (<5%) of  $\text{Ir}_3\text{Te}_8$  (18–20) was present, possibly as a surface impurity. Because  $\text{Ir}_3\text{Te}_8$  is diamagnetic ( $\chi_m = -2.4 \times 10^{-4}$  emu mol<sup>-1</sup>) (20), its presence at this low concentration makes only a small, temperature-independent contribution to the total susceptibility, and no correction was attempted.

Variable-temperature magnetic susceptibility measurements were made from 4.5 to 300 K at a field strength of 5 kG with a Quantum Design SQUID magnetometer. Sample weights were 7 mg for  $\text{NbIrTe}_4$  and 27 mg for  $\text{TaIrTe}_4$ . The magnetic data were corrected for background contributions from the sample holder over the entire temperature range. At 4.5 K, the susceptibilities of both  $\text{NbIrTe}_4$  and  $\text{TaIrTe}_4$  are independent of the magnetic field from 5 to 10 kG.

*Structure determination of  $\text{NbIrTe}_4$ .* Analysis of rotation and Weissenberg photographs of  $\text{NbIrTe}_4$  revealed Laue symmetry mmm and gave preliminary cell parameters. The systematic extinction ( $h0l$ ,  $h + l = 2n + 1$ ) is consistent with the orthorhombic space groups  $D_{2h}^{13}-Pmnm$  and  $C_{2v}^7-Pmn2_1$ . The final cell parameters were determined from a least-squares analysis of the setting angles of 25 reflections in the range  $35^\circ < 2\theta(\text{MoK}\alpha_1) < 45^\circ$ , automatically centered on a Picker diffractometer. Intensity data were collected at 294 K with the  $\theta$ - $2\theta$  technique in the range  $3^\circ \leq 2\theta(\text{MoK}\alpha_1) \leq 60^\circ$  by methods standard in this laboratory (21). Six standard reflections monitored at intervals of every 100 reflections showed no significant change during the course of data collection. Crystal data and further details of the data collection are given in Table I.

All calculations were carried out on a Stardent ST2500 computer with methods and programs standard in this laboratory (21). Conventional atomic scattering factors and anomalous dispersion corrections were taken from the usual sources (22, 23). The intensity data were processed and corrected for absorption effects (24). The initial positions for all atoms were determined by direct methods with the program SHELXS86 (25). A solution with a low combined figure of merit could only be found in the non-centrosymmetric space group  $Pmn2_1$ . This choice of space group was further supported by the fact that  $WTe_2$  (16) also crystallizes in  $Pmn2_1$  in a subcell of  $NbIrTe_4$ . The  $+l$  and  $-l$  reflections were averaged separately, reducing the 7229 measured reflections to 2150 unique reflections with a value for the  $R$ -index for averaging of 0.062. The intensities of the unaveraged  $hkl$  and  $hk\bar{l}$  reflections were

TABLE I  
CRYSTAL DATA AND INTENSITY COLLECTION  
FOR  $NbIrTe_4$

Formula	$NbIrTe_4$
Formula mass (amu)	795.53
Space group	$C_{2v}^7-Pmn2_1$
$a$ (Å)	3.768(3) <sup>a</sup>
$b$ (Å)	12.486(10)
$c$ (Å)	13.077(9)
$V$ (Å <sup>3</sup> )	615.2
$Z$	4
$\rho_c$ (g cm <sup>-3</sup> )	8.59
$T$ of data collection (K)	294
Radiation	Graphite monochromated $MoK\alpha$ ( $\lambda(K\alpha_1) =$ 0.7093 Å)
Crystal shape	Flat needle $0.272 \times$ $0.045 \times 0.004$ mm, bounded by $\{100\}$ , $\{010\}$ , $\{001\}$
Crystal volume (mm <sup>3</sup> )	$4.90 \times 10^{-5}$
Linear abs. coeff. (cm <sup>-1</sup> )	418.3
Transmission factors <sup>b</sup>	0.256–0.846
Detector aperture (mm)	Horizontal, 5.0; vertical, 6.0; 30.5 cm from crystal

TABLE I—Continued

Takeoff angle (deg.)	2.5
Scan type	$\theta$ - $2\theta$
Scan speed (deg. min <sup>-1</sup> )	2.0 in $2\theta$
Scan range (deg.)	1.3 below $K\alpha_1$ to 1.3 above $K\alpha_2$
$\lambda^{-1} \sin \theta$ , limits (Å <sup>-1</sup> )	0.037–0.705, $3^\circ \leq 2\theta(MoK\alpha_1) \leq 60^\circ$
Background counts	10 sec at each end of scan <sup>c</sup>
Data collected	$\pm h, \pm k, \pm l$
$p$ factor	0.04
No. of data collected	7229
No. of unique data, including $F_o^2 < 0$	2150
No. of unique data, with $F_o^2 > 3\sigma(F_o^2)$	1513
No. of variables	36
$R(F^2)$	0.158
$R_w(F^2)$	0.187
$R$ (on $F$ for $F_o^2 > 3\sigma(F_o^2)$ )	0.076
Error in observation of unit weight ( $e^2$ )	2.41

<sup>a</sup> Obtained from a refinement constrained so that  $\alpha = \beta = \gamma = 90^\circ$ .

<sup>b</sup> The analytical method as employed in the Northwestern absorption program, AGNOST, was used for the absorption correction (24).

<sup>c</sup> The diffractometer was operated using the Indiana University PCPS system (50).

compared in order to determine the sense of the polar axis  $z$  of this crystal. Of the 275 reflections for which  $F_c$  differed by more than 5% between the  $hkl$  and  $hk\bar{l}$  reflections, 180 of the differences were accounted for by the chosen sense of the polar axis. The program STRUCTURE TIDY (26) was used to standardize the crystal structure according to rules formulated previously (27).<sup>2</sup> As the four metal sites are very similar, a refinement on  $F_o$  was performed on a model in which each site was allowed to be fully occupied by a mixture of

<sup>2</sup> Although some precedent has been set by the choice of a nonstandard setting ( $Pnm2_1$ ) for the closely related structure of  $WTe_2$  (16), we have opted to adhere to these standardization rules.

Nb and Ir atoms, but no constraint was placed on the overall Nb:Ir ratio. This resulted in occupancies of 100(2)% Nb and 105(2)% Nb in two metal sites, and 99(2)% Ir and 92(2)% Ir in the other two metal sites, with no improvement in the  $R$ -index (0.075) compared to that of a refinement on an ordered model. Thus, we accept the ordered model. The final cycle of isotropic refinement on  $F_o^2$  of 36 variables and 2150 averaged reflections (including those having  $F_o^2 < 0$ ) converged to a value of  $R(F_o^2)$  of 0.158. The value for the conventional  $R$ -index (on  $F$  for  $F_o^2 > 3\sigma(F_o^2)$ ) is 0.076. The final difference electron density map shows no features with a height greater than 5.7% that of an Ir atom. Final values of the atomic parameters and isotropic thermal parameters are given in Table II. The unexceptional nature of the thermal parameters further supports an ordered structure with stoichiometry NbIrTe<sub>4</sub>. Final structure amplitudes are given in Table III.<sup>3</sup>

Weissenberg photography on the compound TaIrTe<sub>4</sub> shows that it is isostructural to NbIrTe<sub>4</sub> with a cell of dimensions  $a = 3.77(3)$ ,  $b = 12.37(6)$ ,  $c = 13.17(3)$  Å at room temperature. Owing to the similarity of the scattering factors of Ta and Ir, it might be difficult to distinguish between them on the basis of conventional X-ray diffraction methods. However, the ordered arrangement of the metal atoms in NbIrTe<sub>4</sub> lends support to a similar arrangement in TaIrTe<sub>4</sub>.

<sup>3</sup> See NAPS document No. 04902 for 10 pages of supplementary materials. Order from ASIS/NAPS, Microfiche Publications, P.O. Box 3513, Grand Central Station, New York, NY 10163-3513. Remit in advance \$4.00 for microfiche copy or for photocopy, \$7.75. All orders must be prepaid. Institutions and Organizations may order by purchase order. However, there is a billing and handling charge for this service of \$15. Foreign orders add \$4.50 for postage and handling, \$1.75 for postage of any microfiche orders.

TABLE II  
POSITIONAL PARAMETERS AND ISOTROPIC THERMAL  
PARAMETERS FOR NbIrTe<sub>4</sub>

Atom	Wyckoff position	x	y	z	$B(\text{Å}^2)$
Nb(1)	2a	0	0.0545(3)	0.0050(5)	0.36(7)
Nb(2)	2a	0	0.2693(4)	0.4923(6)	0.68(7)
Ir(1)	2a	0	0.5359(1)	0	0.24(3)
Ir(2)	2a	0	0.7520(1)	0.4921(2)	0.16(3)
Te(1)	2a	0	0.0648(3)	0.3894(4)	0.40(5)
Te(2)	2a	0	0.1956(3)	0.8527(3)	0.32(5)
Te(3)	2a	0	0.3472(2)	0.0961(3)	0.24(5)
Te(4)	2a	0	0.4135(3)	0.6394(4)	0.55(6)
Te(5)	2a	0	0.5631(3)	0.3959(3)	0.26(5)
Te(6)	2a	0	0.6764(3)	0.8464(4)	0.44(5)
Te(7)	2a	0	0.8512(2)	0.1095(3)	0.38(5)
Te(8)	2a	0	0.8900(3)	0.6494(3)	0.37(5)

Note.  $B = 8\pi^2u^2$ .

## Results

*Description of the structure.* Selected interatomic distances and angles for NbIrTe<sub>4</sub> are given in Table IV. A view down the  $a$  axis, given in Fig. 1, shows the labeling scheme and the layer stacking. A view down the  $c$  axis, given in Fig. 2, shows an individual layer. The compound NbIrTe<sub>4</sub>

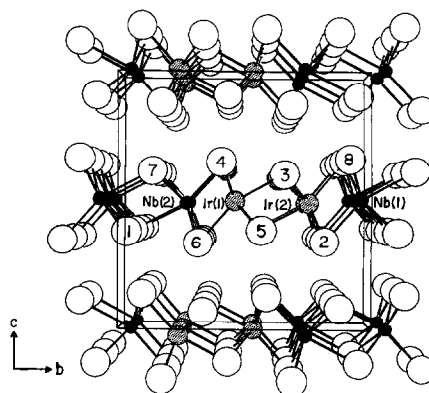


FIG. 1. View of NbIrTe<sub>4</sub> down the  $a$  axis showing the labeling scheme and unit cell outline. The small solid circles are Nb atoms, the medium stippled circles are Ir atoms, and the large open circles are Te atoms.

TABLE IV  
SELECTED INTERATOMIC DISTANCES (Å) AND  
ANGLES (DEG.) FOR NbIrTe<sub>4</sub>

Nb(1)-Te(2)	2.659(6)	Te(1)-2Te(7)	3.597(4)
Nb(1)-2Te(8)	2.755(5)	Te(1)-2Te(8)	3.704(5)
Nb(1)-2Te(1)	2.838(5)	Te(1)-2Te(1)	3.768(3)
Nb(1)-Te(7)	2.883(6)	Te(1)-2Te(6)	3.783(5)
Nb(1)-2Ir(2)	3.068(4)	Te(1)-2Te(2)	3.788(5)
Nb(1)-2Nb(1)	3.768(3)	Te(2)-2Te(5)	3.598(4)
		Te(2)-Te(3)	3.704(5)
Nb(2)-Te(4)	2.636(7)	Te(2)-2Te(7)	3.742(5)
Nb(2)-2Te(6)	2.765(5)	Te(2)-2Te(2)	3.768(3)
Nb(2)-2Te(7)	2.857(5)	Te(2)-Te(4)	3.896(5)
Nb(2)-Te(1)	2.886(6)	Te(3)-2Te(5)	3.415(4)
Nb(2)-2Ir(1)	3.078(5)	Te(3)-2Te(4)	3.577(5)
Nb(2)-2Nb(2)	3.768(3)	Te(3)-2Te(8)	3.579(4)
		Te(3)-2Te(3)	3.768(3)
Ir(1)-2Te(5)	2.633(3)	Te(3)-2Te(6)	3.787(5)
Ir(1)-Te(6)	2.667(5)	Te(4)-Te(5)	3.692(6)
Ir(1)-Te(3)	2.671(4)	Te(4)-2Te(4)	3.768(3)
Ir(1)-2Te(4)	2.697(4)	Te(4)-2Te(7)	3.824(5)
Ir(1)-2Ir(1)	3.768(3)	Te(4)-2Te(5)	3.858(5)
		Te(5)-2Te(6)	3.594(4)
Ir(2)-2Te(3)	2.634(3)	Te(5)-2Te(5)	3.768(3)
Ir(2)-Te(5)	2.673(4)	Te(6)-Te(8)	3.708(5)
Ir(2)-Te(8)	2.684(4)	Te(6)-2Te(6)	3.768(3)
Ir(2)-2Te(2)	2.702(3)	Te(7)-2Te(7)	3.768(3)
Ir(2)-2Ir(2)	3.768(3)	Te(7)-2Te(8)	3.777(5)
		Te(8)-2Te(8)	3.768(3)
Te(7)-Nb(1)-Te(8)	84.1(2)	Te(3)-Ir(1)-Te(4)	83.6(1)
Te(7)-Nb(1)-Te(1)	77.9(1)	Te(3)-Ir(1)-Te(5)	80.2(1)
Te(2)-Nb(1)-Te(8)	110.3(1)	Te(6)-Ir(1)-Te(4)	110.8(1)
Te(2)-Nb(1)-Te(1)	87.0(2)	Te(6)-Ir(1)-Te(5)	85.4(1)
Te(8)-Nb(1)-Te(1)	92.5(1)	Te(4)-Ir(1)-Te(5)	87.7(1)
Te(8)-Nb(1)-Te(8)	86.3(2)	Te(4)-Ir(1)-Te(4)	88.6(1)
Te(1)-Nb(1)-Te(1)	83.2(2)	Te(5)-Ir(1)-Te(5)	91.4(1)
Ir(2)-Nb(1)-Ir(2)	75.8(1)	Nb(2)-Ir(1)-Nb(2)	75.5(1)
Te(1)-Nb(2)-Te(6)	84.0(2)	Te(5)-Ir(2)-Te(2)	84.0(1)
Te(1)-Nb(2)-Te(7)	77.5(1)	Te(5)-Ir(2)-Te(3)	80.1(1)
Te(4)-Nb(2)-Te(6)	109.7(2)	Te(8)-Ir(2)-Te(2)	111.2(1)
Te(4)-Nb(2)-Te(7)	88.1(2)	Te(8)-Ir(2)-Te(3)	84.6(1)
Te(6)-Nb(2)-Te(7)	92.9(1)	Te(2)-Ir(2)-Te(3)	87.9(1)
Te(6)-Nb(2)-Te(6)	85.9(2)	Te(2)-Ir(2)-Te(2)	88.4(1)
Te(7)-Nb(2)-Te(7)	82.5(2)	Te(3)-Ir(2)-Te(3)	91.3(1)
Ir(1)-Nb(2)-Ir(1)	75.5(1)	Nb(1)-Ir(2)-Nb(1)	75.8(1)

has a layered structure closely related to those of WTe<sub>2</sub> and β-MoTe<sub>2</sub> (16). The Nb and Ir atoms are octahedrally coordinated by Te atoms. Although the Te atoms are not strictly close-packed, the order of the stacking of anion layers may be described as (ABAC) or (hc) (28). Thus, the structure represents a variant of the CdI<sub>2</sub> type (29). However, the Te layers are severely buckled as a result of displacements of the Nb and Ir atoms out of the ideal octahedral sites. As occurs in the WTe<sub>2</sub> and β-MoTe<sub>2</sub>

structures (16), this buckling requires the Te layers to stack in a manner such that crests fit into troughs across the van der Waals' gap and vice versa. Note that the metal atoms are ordered. The Nb and Ir atoms can be regarded each as forming chains of edge-sharing octahedra extending along the *a* direction. The chains are then linked to form an individual layer, ordering in the fashion [...Nb-Ir...Ir-Nb...], as seen in Fig. 1. Each metal atom closely approaches two neighboring metal atoms of the other kind in the adjacent chain, forming a zigzag chain that extends along the *a* direction, as seen in Fig. 2. This feature is also observed in WTe<sub>2</sub> and β-MoTe<sub>2</sub> and has been attributed to the occurrence of metal-metal bonding. It is unclear why the chains in NbIrTe<sub>4</sub> should order in the particular manner shown and not, for example, as [...Nb-Ir...Nb-Ir...].

The structure of NbIrTe<sub>4</sub> is thus an ordered variant of the WTe<sub>2</sub> and β-MoTe<sub>2</sub> structures (16), which are unique among those that occur in the transition-metal dichalcogenides. The sulfides and selenides of molybdenum and tungsten occur in MoS<sub>2</sub> polytypes in which the metal has trigonal prismatic coordination, whereas distorted

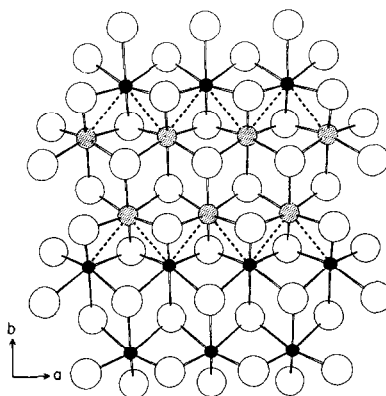


FIG. 2. View of NbIrTe<sub>4</sub> down the *c* axis showing an individual layer and the zigzag metal chains extending along the *a* direction. Atoms are as marked in Fig. 1.

TABLE V  
COMPARISON OF IMPORTANT INTERATOMIC DISTANCES (Å) IN NbIrTe<sub>4</sub>, β-MoTe<sub>2</sub>, AND WTe<sub>2</sub>

	NbIrTe <sub>4</sub>	β-MoTe <sub>2</sub> <sup>a</sup>	WTe <sub>2</sub> <sup>a</sup>
Range of M–Te	2.636(7)–2.866(6) (Nb–Te) 2.633(3)–2.702(3) (Ir–Te)	2.701(6)–2.816(7)	2.708(5)–2.820(7)
Range of short M–M'	3.068(4)–3.078(5) (Nb–Ir)	2.895(8)–2.901(9)	2.861(4)
Shortest Te–Te			
Intralayer <sup>b</sup>	3.415(4) (Te(3)–Te(5))	3.469	3.496
Interlayer <sup>c</sup>	3.704(5) (Te(1)–Te(8))	3.855(5)	3.927(8)

<sup>a</sup> Ref. (16).

<sup>b</sup> Within the Te–M–Te sandwiches.

<sup>c</sup> Across the van der Waals' gap.

octahedral coordination occurs in the tellurides (30–33). The particular ordering of the Nb and Ir atoms in NbIrTe<sub>4</sub> necessitates a doubling of the unit cell compared to that of WTe<sub>2</sub>. The compound β-MoTe<sub>2</sub> adopts a monoclinic distortion ( $\beta = 93.92^\circ$ ) of this orthorhombic structure (16). The distortion occurs because of a slight shifting of the Te layers. Indeed, there is some evidence that β-MoTe<sub>2</sub> undergoes a phase transition in which the  $\beta$  angle decreases to  $90^\circ$  (34, 35). A structure related to the WTe<sub>2</sub>-type is that of NbTe<sub>2</sub> and TaTe<sub>2</sub> (15), which displays a similar distortion of the metal octahedra that are now grouped into *triple* metal-bonded chains.

It is interesting to compare various interatomic distances among NbIrTe<sub>4</sub>, β-MoTe<sub>2</sub>, and WTe<sub>2</sub> (Table V). In NbIrTe<sub>4</sub>, the range of Nb–Te distances is comparable to that found in NbTe<sub>2</sub> (2.690(7)–2.908(7) Å) (15), and similarly the range of Ir–Te distances is comparable to that found in IrTe<sub>2</sub> (2.650 Å) (18, 19, 36) and Ir<sub>3</sub>Te<sub>8</sub> (2.652(3)–2.655(2) Å) (18–20). The M–Te distances in β-MoTe<sub>2</sub> and WTe<sub>2</sub> lie in the same range (16). The metal–metal distances in the zigzag chains of these compounds are slightly longer than those found in the elemental metals. In β-MoTe<sub>2</sub>, the Mo–Mo distance (2.895(8) Å) exceeds that in molybdenum metal (2.7254(3) Å) (37) by

0.170(8) Å; in WTe<sub>2</sub>, the W–W distance (2.861(4) Å) exceeds that in tungsten metal (2.7411(3) Å) (37) by 0.120(4) Å; in NbIrTe<sub>4</sub>, the Nb–Ir distance (3.068(4) Å) exceeds the average of the metal–metal distances in niobium and iridium metals (2.8585(3) and 2.7147(3) Å, respectively, (37)) by 0.281(4) Å. These distances and the distortion of the metal positions from the ideal octahedral sites indicate the presence of some degree of metal–metal bonding. This feature has also been observed in other tellurides of niobium and tantalum (e.g., NbTe<sub>2</sub> (15), TaTe<sub>2</sub> (15, 38), Ta<sub>3</sub>Pd<sub>3</sub>Te<sub>14</sub> (11), Ta<sub>4</sub>Pd<sub>3</sub>Te<sub>16</sub> (6)) as well as in other transition-metal chalcogenides where the metals have distorted octahedral geometries (39). The origin of this "metal clustering," as it has been termed, was probed by tight-binding electronic band structure calculations for *d*<sup>2</sup> and *d*<sup>3</sup> metal ions, and was clearly linked to metal–metal bond formation (39, 40). Finally, the Te–Te distances in NbIrTe<sub>4</sub> are generally shorter than those in β-MoTe<sub>2</sub> and WTe<sub>2</sub> (16); many range from 3.4 to 3.8 Å (Table IV). While these distances are much longer than a full Te–Te single bond, such as that found in HfTe<sub>5</sub> (2.763(4) Å) (41), they are shorter than an ionic Te<sup>2-</sup>–Te<sup>2-</sup> separation (4.2 Å) (42), indicating that intermediate Te–Te interactions are prevalent here. The shortest Te–

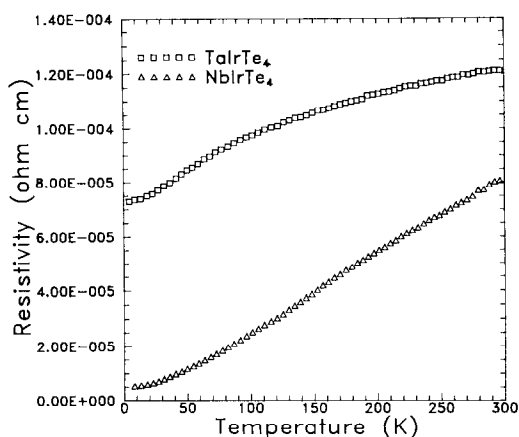


FIG. 3. Plots of electrical resistivity vs. temperature along the needle axis  $a$  for single crystals of NbIrTe<sub>4</sub> and TaIrTe<sub>4</sub>.

Te distance across the van der Waals' gap has decreased to 3.704(5) Å in NbIrTe<sub>4</sub>, indicating that interlayer interactions are stronger here than in β-MoTe<sub>2</sub> and WTe<sub>2</sub>. Thus the structure of NbIrTe<sub>4</sub> may be described alternatively as containing an extensive network of weakly-bonded Te atoms.

**Electrical resistivity and magnetic susceptibility.** Plots of the electrical resistivity along the needle axis  $a$  as a function of temperature are shown in Fig. 3 for NbIrTe<sub>4</sub> and TaIrTe<sub>4</sub>. Both compounds are metallic, with NbIrTe<sub>4</sub> being a better conductor than TaIrTe<sub>4</sub> by about an order of magnitude. The resistivity vs temperature curve is also flatter for TaIrTe<sub>4</sub> ( $\rho_{298}/\rho_5 = 1.6$ ) than for NbIrTe<sub>4</sub> ( $\rho_{298}/\rho_5 = 15$ ). Plots of the molar magnetic susceptibility as a function of temperature are shown in Fig. 4. The measured susceptibilities of NbIrTe<sub>4</sub> and TaIrTe<sub>4</sub> are  $1.6 \times 10^{-3}$  and  $5.6 \times 10^{-4}$  emu mol<sup>-1</sup>, respectively. If one assumes that contributions from ion-core diamagnetism originate from Nb<sup>5+</sup>, Ta<sup>5+</sup>, Ir<sup>3+</sup>, and Te<sup>2-</sup> (43), then the corrected susceptibilities for NbIrTe<sub>4</sub> and TaIrTe<sub>4</sub> are  $1.9 \times 10^{-3}$  and  $8.9 \times 10^{-4}$  emu mol<sup>-1</sup>, respectively. The

susceptibilities of both compounds are essentially temperature-independent, consistent with Pauli paramagnetism expected for metals. The susceptibility of NbIrTe<sub>4</sub> is slightly greater than that of TaIrTe<sub>4</sub> and shows a slight increase at low temperature (below 20 K).

Table VI compares the values of electrical resistivity and magnetic susceptibility of NbIrTe<sub>4</sub>, TaIrTe<sub>4</sub>, β-MoTe<sub>2</sub>, and WTe<sub>2</sub>. All these compounds are metallic and Pauli paramagnetic. There appears to be a trend in which the compounds become more conducting (less resistive) and more magnetic in the order WTe<sub>2</sub> < β-MoTe<sub>2</sub> < TaIrTe<sub>4</sub> < NbIrTe<sub>4</sub>. This observation would be consistent with the idea that Pauli paramagnetism arises from the conduction electrons whose magnitude is proportional to the density of states at the Fermi level (44, 45), although no electronic band structure calculation is yet available for NbIrTe<sub>4</sub>. However, the band structures of β-MoTe<sub>2</sub> (40, 46) and WTe<sub>2</sub> (46) have been calculated. If we attempt to assign oxidation states to the metal atoms in NbIrTe<sub>4</sub>, the only reasonable choices are

- (i) Nb<sup>5+</sup> ( $d^0$ ) and Ir<sup>3+</sup> ( $d^6$ ), or
- (ii) Nb<sup>4+</sup> ( $d^1$ ) and Ir<sup>4+</sup> ( $d^5$ ).

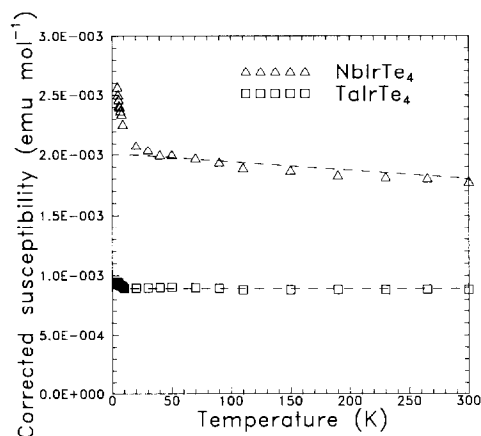


FIG. 4. Plots of molar magnetic susceptibility vs. temperature for NbIrTe<sub>4</sub> and TaIrTe<sub>4</sub> at 5 kG.

TABLE VI  
ELECTRICAL RESISTIVITY AND MAGNETIC SUSCEPTIBILITY OF  $M\text{IrTe}_4$  ( $M = \text{Nb, Ta}$ ),  $\text{WTe}_2$ ,  
AND  $\beta\text{-MoTe}_2$

Compound	$\rho_{298}$ ( $\Omega \text{ cm}$ ) <sup>a</sup>	$\rho_5$ ( $\Omega \text{ cm}$ ) <sup>a</sup>	$\chi_m$ ( $\text{emu mol}^{-1}$ ) <sup>b</sup>	Reference
$\text{NbIrTe}_4$	$8.1 \times 10^{-5}$	$5.3 \times 10^{-6}$	$1.9 \times 10^{-3}$	This work
$\text{TaIrTe}_4$	$1.2 \times 10^{-4}$	$7.7 \times 10^{-5}$	$8.9 \times 10^{-4}$	This work
$\beta\text{-MoTe}_2$	$5.6 \times 10^{-4}$	$5 \times 10^{-5}$	$2.3 \times 10^{-4}$	(16, 48, 49, 52)
$\text{WTe}_2$	$7 \times 10^{-4}$	$1 \times 10^{-4}$	— <sup>c</sup>	(16, 47, 51, 52)

<sup>a</sup> Measured along the needle axis of single crystals.

<sup>b</sup> The compounds show temperature-independent Pauli paramagnetism.

<sup>c</sup> No values have been found in the literature.

Arguments can be provided for preferring one over the other: the alternation of Nb and Ir atoms in the metal chains as well as the stability of  $\text{Ir}^{3+}$  favors choice (i), while the existence of some metal–metal bonding and a more equitable distribution of charge favors choice (ii). In reality, the situation is probably intermediate between the two. Moreover, the prevalence of  $\text{Te}\cdots\text{Te}$  interactions suggests that tellurium is very unlikely to bear its full oxidizing power, and consequently the charges on the metal atoms are probably much lower. In any case, some predictions can be made if we note that there are a total of six  $d$  electrons per formula unit of  $\text{NbIrTe}_4$ , compared to only four  $d$  electrons per formula unit of  $\text{Mo}_2\text{Te}_4$  or  $\text{W}_2\text{Te}_4$ . The band structures of  $\beta\text{-MoTe}_2$  and  $\text{WTe}_2$  are very similar and show considerable dispersion arising from intimate mixing of the metal  $d$  and tellurium  $p$  orbitals (46). The Fermi levels of  $\beta\text{-MoTe}_2$  and  $\text{WTe}_2$  lie in deep troughs in the density of states (DOS) vs energy curve, leading to values of electrical conductivity in the semimetallic regime (47–49). We can assume that the gross band structure of  $\text{NbIrTe}_4$  differs little from those of  $\beta\text{-MoTe}_2$  and  $\text{WTe}_2$ , despite the doubling of the unit cell and the substitution of the transition metals. With more electrons available in  $\text{NbIrTe}_4$ , the bands fill up beyond the trough in the DOS curve, and so the DOS is

greater at the Fermi level here than in  $\beta\text{-MoTe}_2$  and  $\text{WTe}_2$ , consistent with the trends observed in the physical properties (vide supra).

The compounds  $\text{NbIrTe}_4$  and  $\text{TaIrTe}_4$  may belong to a larger class of compounds with the general formula  $MM'\text{Te}_4$  ( $M = \text{Nb, Ta}$ ;  $M' = \text{Ru, Os, Rh, Ir}$ ). From preliminary X-ray powder diffraction and Weissenberg data, the compounds  $\text{TaRuTe}_4$ ,  $\text{NbOsTe}_4$ , and  $\text{TaRhTe}_4$  appear to be isostructural or closely related to  $\text{NbIrTe}_4$ . We are presently engaged in synthesizing the other members of this series with an interest in comparing their physical properties and in understanding their electronic band structures.

### Acknowledgments

This work was supported by the U.S. National Science Foundation through Grant DMR-88-09854 (Science and Technology Center for Superconductivity) and Grant DMR-88-13623. Use was made of the SEM, electrical conductivity, and magnetic susceptibility facilities of the Materials Research Center at Northwestern University (U.S. National Science Foundation Grant DMR-88-21571).

### References

1. P. BÖTTCHER, *Angew. Chem. Int. Ed. Engl.* **27**, 759 (1988).
2. M. E. BADDING AND F. J. DISALVO, *Inorg. Chem.* **29**, 3952 (1990).

3. P. M. KEANE AND J. A. IBERS, *Inorg. Chem.* **30**, 1327 (1991).
4. P. M. KEANE AND J. A. IBERS, *J. Solid State Chem.* **93**, 291 (1991).
5. E. W. LIIMATTA AND J. A. IBERS, *J. Solid State Chem.* **71**, 384 (1987).
6. A. MAR AND J. A. IBERS, *J. Chem. Soc. Dalton Trans.* 639 (1991).
7. B. HUANG, J. HUANG, AND S. LIU, *Jiegou Huaxue* **8**, 145 (1989).
8. J. HUANG AND B. HUANG, *Jiegou Huaxue* **7**, 214 (1988).
9. S. A. SUNSHINE, D. A. KEZSLER, AND J. A. IBERS, *Acc. Chem. Res.* **20**, 395 (1987).
10. A. MAR AND J. A. IBERS, *J. Solid State Chem.* **92**, 352 (1991).
11. E. W. LIIMATTA AND J. A. IBERS, *J. Solid State Chem.* **78**, 7 (1989).
12. E. W. LIIMATTA AND J. A. IBERS, *J. Solid State Chem.* **77**, 141 (1988).
13. K. HAYASHI, M. HYOMA, H. YAMANAKA, AND H. NISHIHARA, *J. Less-Common Met.* **147**, 19 (1989).
14. F. HULLIGER, in "Physics and Chemistry of Materials with Layered Structures, 5: Structural Chemistry of Layer-Type Phases" (F. Lévy, Ed.), pp. 234–242, D. Reidel, Dordrecht, Holland (1976).
15. B. E. BROWN, *Acta Crystallogr.* **20**, 264 (1966).
16. B. E. BROWN, *Acta Crystallogr.* **20**, 268 (1966).
17. T. E. PHILLIPS, J. R. ANDERSON, C. J. SCHRAMM, AND B. M. HOFFMAN, *Rev. Sci. Instrum.* **50**, 263 (1979).
18. E. F. HOCKINGS AND J. G. WHITE, *J. Phys. Chem.* **64**, 1042 (1960).
19. SUTARNO, O. KNOP, AND K. I. G. REID, *Can. J. Chem.* **45**, 1391 (1967).
20. S. JOBIC, M. EVAIN, R. BREC, P. DENIARD, A. JOUANNEAUX, AND J. ROUXEL, *J. Solid State Chem.* **95**, 319 (1991).
21. J. M. WATERS AND J. A. IBERS, *Inorg. Chem.* **16**, 3273 (1977).
22. D. T. CROMER AND J. T. WABER, in "International Tables for X-ray Crystallography" (J. A. Ibers and W. C. Hamilton, Eds.), Vol. 4, Table 2.2A, pp. 72–98, Kynoch Press, Birmingham, England (1974).
23. D. T. CROMER, in "International Tables for X-ray Crystallography" (J. A. Ibers and W. C. Hamilton, Eds.), Vol. 4, Table 2.3.1, pp. 149–150, Kynoch Press, Birmingham, England (1974).
24. J. DE MEULENAER AND H. TOMPA, *Acta Crystallogr.* **19**, 1014 (1965).
25. G. M. SHELDRICK, in "Crystallographic Computing 3," (G. M. Sheldrick, C. Krüger, and R. Goddard, Eds.), pp. 175–189, Oxford Univ. Press, Oxford (1985).
26. L. M. GELATO AND E. PARTHÉ, *J. Appl. Crystallogr.* **20**, 139 (1987).
27. E. PARTHÉ AND L. M. GELATO, *Acta Crystallogr., Sect. A: Found. Crystallogr.* **40**, 169 (1984).
28. F. HULLIGER, in "Physics and Chemistry of Materials with Layered Structures, 5: Structural Chemistry of Layer-Type Phases" (F. Lévy, Ed.), pp. 230–232, D. Reidel, Dordrecht, Holland (1976).
29. A. F. WEISS, "Structural Inorganic Chemistry," 5th ed., pp. 258–265, Clarendon Press, Oxford (1984).
30. A. A. BALCHIN, in "Physics and Chemistry of Materials with Layered Structures, 2: Crystallography and Crystal Chemistry of Materials with Layered Structures" (F. Lévy, Ed.), pp. 1–50, D. Reidel, Dordrecht, Holland (1976).
31. F. R. GAMBLE, *J. Solid State Chem.* **9**, 358 (1974).
32. R. HUISMAN, R. DE JONGE, C. HAAS, AND F. JELLINEK, *J. Solid State Chem.* **3**, 56 (1971).
33. B. F. MENTZEN AND M. J. SIENKO, *Inorg. Chem.* **15**, 2198 (1976).
34. C. MANOLIKAS, J. VAN LANDUYT, AND S. AMELINCKX, *Phys. Status Solidi A* **53**, 327 (1979).
35. R. CLARKE, E. MARSEGLIA, AND H. P. HUGHES, *Philos. Mag. B* **38**, 121 (1978).
36. S. JOBIC, P. DENIARD, R. BREC, J. ROUXEL, A. JOUANNEAUX, AND A. N. FITCH, *Z. Anorg. Allg. Chem.* **598/599**, 199 (1991).
37. J. DONOHUE, "The Structures of the Elements," Wiley-Interscience, New York (1974).
38. S. LEE AND N. NAGASUNDARAM, *Chem. Mater.* **1**, 597 (1989).
39. E. CANADELL, A. LEBEUZE, M. A. EL KHALIFA, R. CHEVREL, AND M.-H. WHANGBO, *J. Am. Chem. Soc.* **111**, 3778 (1989).
40. E. CANADELL AND M.-H. WHANGBO, *Inorg. Chem.* **29**, 1398 (1990).
41. S. FURUSETH, L. BRATTÅS, AND A. KJEKSHUS, *Acta Chem. Scand.* **27**, 2367 (1973).
42. R. D. SHANNON, *Acta Crystallogr., Sect. A: Cryst. Phys. Diff. Theor. Gen. Crystallogr.* **32**, 751 (1976).
43. L. N. MULAY AND E. A. BOUDREAUX, Eds., "Theory and Applications of Molecular Diamagnetism," Wiley-Interscience, New York (1976).
44. N. W. ASHCROFT AND N. D. MERMIN, "Solid State Physics," pp. 661–664, Saunders College, Philadelphia (1976).
45. P. A. COX, "The Electronic Structure and Chemistry of Solids," pp. 67–68, Oxford Univ. Press, Oxford (1987).
46. W. G. DAWSON AND D. W. BULLETT, *J. Phys. C: Solid State Phys.* **20**, 6159 (1987).

47. S. KABASHIMA, *J. Phys. Soc. Jpn.* **21**, 945 (1966).
48. H. P. HUGHES AND R. H. FRIEND, *J. Phys. C: Solid State Phys.* **11**, L103 (1978).
49. M. B. VELLINGA, R. DE JONGE, AND C. HAAS, *J. Solid State Chem.* **2**, 299 (1970).
50. J. C. HUFFMAN, unpublished work.
51. L. H. BRIXNER, *J. Inorg. Nucl. Chem.* **24**, 257 (1962).
52. J. M. VANDENBERG-VOORHOEVE, in "Physics and Chemistry of Materials with Layered Structures, 4: Optical and Electrical Properties" (P. A. Lee, Ed.), p. 426, D. Reidel, Dordrecht, Holland (1976).